Invited Paper

InAlGaN optical emitters – laser diodes with non-epitaxial cladding layers and ultraviolet light-emitting diodes

Christopher Chua, Zhihong Yang, Clifford Knollenberg, Mark Teepe, Bowen Cheng, Andre Strittmatter, David Bour, and Noble M. Johnson

Palo Alto Research Center, 3333 Coyote Hill Road, Palo Alto, CA 94304, USA

ABSTRACT

We describe recent work on InGaN lasers and AlGaN UV LEDs at the Palo Alto Research Center (PARC). The presentation includes results from InGaN laser diodes in which the usual epitaxial upper cladding layer is replaced with an evaporated or sputtered non-epitaxial material, such as indium tin oxide, silver, or a silver-palladium-copper alloy [1, 2]. Non-epitaxial cladding layers offer several advantages to long wavelength InGaN laser diodes, such as eliminating the need to expose vulnerable InGaN active layers to the high temperatures required for growing conventional p-AlGaN cladding layers subsequent to the active layer growth.

The presentation also discusses our recent results on AlGaN UV LEDs. UV LEDs with 300 micron square geometries operating at λ = 325 nm exhibit output powers of 13 mW with differential quantum efficiencies of 0.054 W/A measured under wafer-level, unpackaged condition with no heat sink. LEDs operating at λ = 290 nm under similar test conditions display output powers of 1.6 mW for large-area 300 μm X 1 mm devices.

Keywords: cladding, UV LED, nitride, laser diode

1. LASER DIODES WITH NON-EPITAXIAL CLADDING

Semiconductor laser diodes (LD) typically use lattice-matched epitaxial layers as waveguide cladding materials. We describe a new laser diode architecture in which the upper cladding layer is replaced with an evaporated or sputtered non-epitaxial material. We demonstrate the concept on 415 nm InGaN laser diodes that use indium tin oxide, silver, or a silver-palladium-copper alloy as the cladding material, chosen because the materials exhibit requisite optical and electrical properties. Figure 1 shows an illustration of the concept.

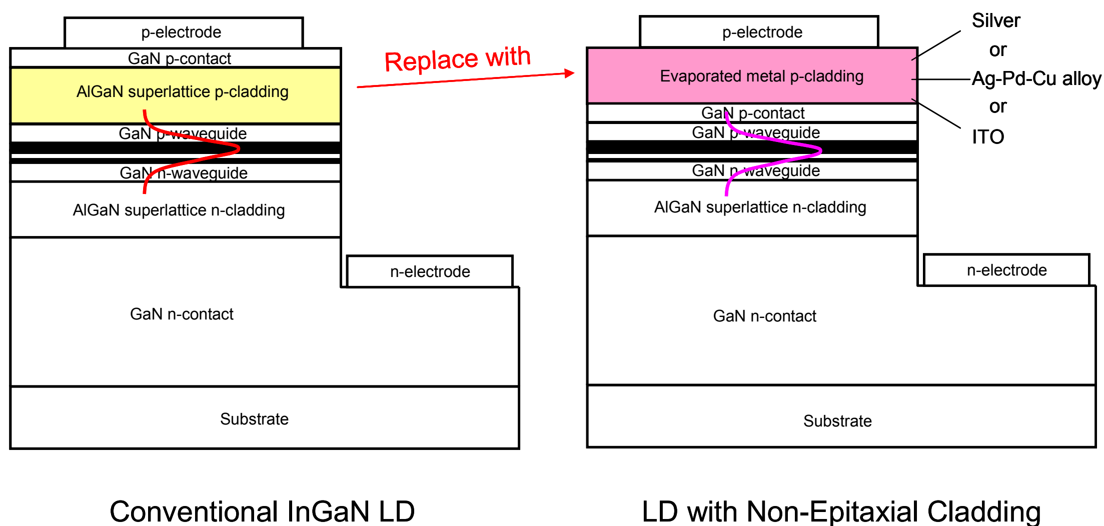

Figure 1: Illustration of laser diode utilizing non-epitaxial cladding layers.

Gallium Nitride Materials and Devices VI, edited by Jen-Inn Chyi, Yasushi Nanishi,
Hadis Morkoç, Joachim Piprek, Euijoon Yoon, Proc. of SPIE Vol. 7939, 793918 · © 2011
SPIE · CCC code: 0277-786X/11/$18 · doi: 10.1117/12.875188

The non-epitaxial cladding layer offers several advantages. It eliminates the need to expose vulnerable InGaN active layers to the high temperatures required for growing conventional p-AlGaN cladding layers subsequent to the active layer growth. The non-epitaxial cladding layer also solves the cracking issues associated with thick, tensile strained AlGaN cladding layers. The non-epitaxial cladding layers are much more electrically conductive than p-doped AlGaN layers, so the alternative cladding layers improve current spreading. Non-epitaxial cladding layers confine the optical mode tightly to the active region and can provide high modal gain. Moreover, the non-epitaxial cladding layer can be easily patterned relative to the underlying layers by selective area deposition or by selective wet etching. This selective patterning capability adds device processing flexibility.

We found that ITO exhibits unique optical and electrical properties that made it a suitable candidate for a cladding material. Figure 2 shows an ITO-clad nitride LD structure along with the calculated optical mode profile. The fundamental transverse mode is asymmetrically biased away from the p-doped layers. This asymmetric modal profile is partly a consequence of the large refractive index step between GaN and ITO and is beneficial for reducing optical losses in the p-doped layers.

The heterostructure was grown on a sapphire substrate by Metal Organic Chemical Vapor Deposition (MOCVD). The first layer was a 4.5 µm-thick Si-doped GaN n-contact layer. The lower cladding layer consisted of an n-doped 680 nm-thick $Al_{0.07}Ga_{0.93}N$ superlattice. An undoped 150 nm-thick waveguide layer was grown above the lower cladding layer, followed by a four-pair multiple quantum well (MQW) active region. The quantum wells were 3 nm-thick $In_{0.1}Ga_{0.9}N$, and the barriers were 6 nm-thick GaN. Next, a 15 nm-thick Mg-doped $Al_{0.18}Ga_{0.82}N$ electron blocking layer was grown, followed by a 240 nm-thick p-waveguide. The lower and upper waveguides, together with the sandwiched MQW region, formed a separate confinement heterostructure (SCH). The SCH was designed to position the optical mode for strong overlap with the gain region, while maintaining acceptable modal loss. A thin 20 nm-thick p+-doped GaN was then grown above the SCH to cap the heterostructure.

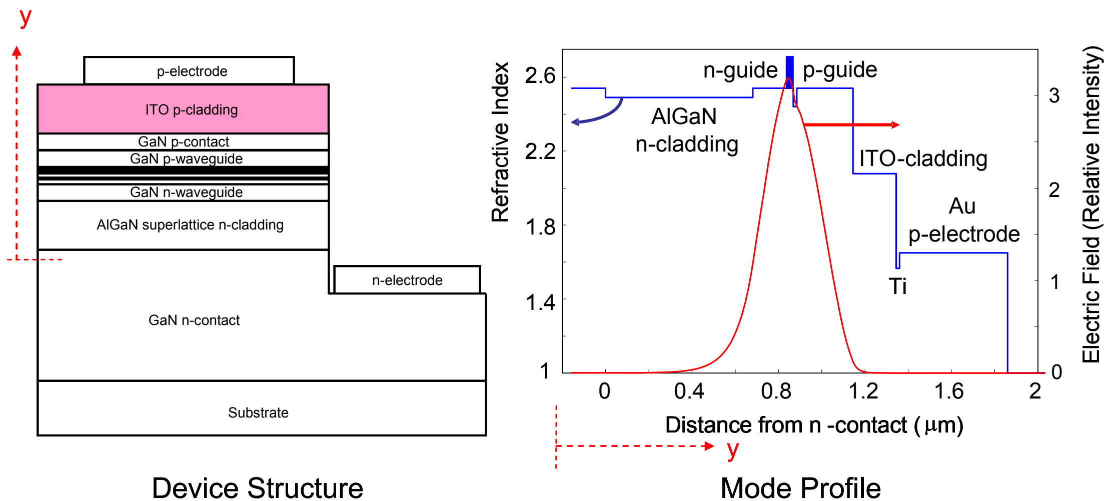

Figure 2: ITO-clad laser diode structure.

Unlike conventional LD structures, our device was grown without an upper p-cladding AlGaN layer. Instead, a 200 nm-thick ITO film was deposited by RF sputtering after the heterostructure growth to form the upper cladding layer. ITO is an attractive upper cladding material because it has a low refractive index and can exhibit low optical loss when deposited under the appropriate sputter conditions. The low refractive index enables an ITO-clad LD structure to provide better optical mode confinement than a conventional structure employing AlGaN:Mg cladding layers. The improved confinement leads to a higher modal gain and to a lower loss due to reduced electric field overlap with the absorbing top-metal electrodes.

ITO is also significantly less resistive than conventional AlGaN:Mg cladding layers and works well as a contact material to p-GaN. It is widely used as an electrical current spreading layer in blue GaN LEDs. In our device, the ITO layer functions simultaneously as a waveguide cladding layer, a current spreading layer, and a p-contact material.

Employing ITO as an upper cladding layer has the additional benefit of simplifying fabrication of ridge waveguide laser diodes. When forming the ridge structures in these devices, conventional AlGaN:Mg cladding layers must be dry etched with no selectivity to the underlying waveguide layer. Therefore, special steps must be taken to prevent damage to the underlying waveguide layer during etching. Unlike AlGaN, ITO can be easily etched by wet chemical means. The process is selective relative to GaN, so the ITO cladding layer can be readily patterned without affecting the underlying heterostructure.

Figure 3 plots the optical confinement factor (Γ) and modal loss (α) of our ITO-clad laser as a function of ITO cladding thickness. For simplicity, only absorption at the ITO-cladding layer and at the Ti/Au metal electrode were included in the definition of α. The p-layer losses were neglected. At our designed ITO cladding thickness of 200 nm, the loss due to metal absorption is only α = 2.1 cm-1, while the optical confinement factor Γ remains nearly constant at about 4% for a wide range of ITO thicknesses.

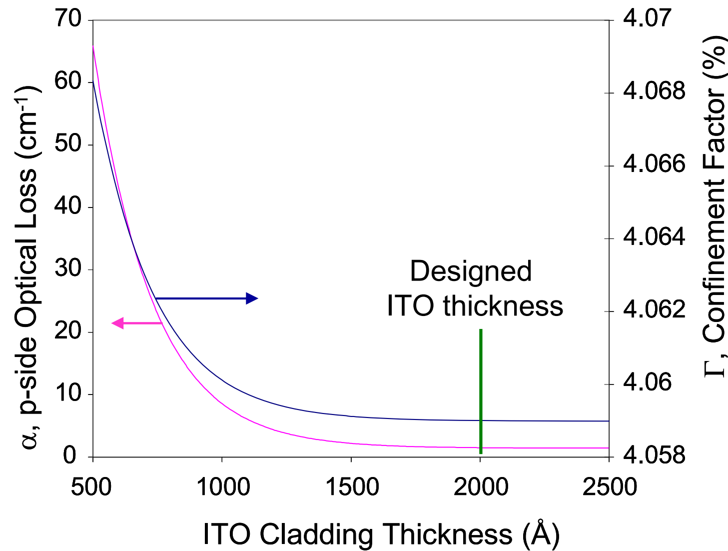

Figure 3: Modal loss and optical confinement factor vs ITO cladding thickness.

The ITO film was deposited under carefully chosen sputter conditions of oxygen partial pressure, sputter power, and ambient pressure to attain an optimized trade-off between film transparency and electrical conductivity. The real and imaginary parts of the refractive index at different wavelengths were determined with multi-wavelength, multi-angle ellipsometry, and these values were used in the device simulations. Figure 4 shows the optical properties of two ITO films deposited under different conditions. The properties depend significantly on deposition conditions, and care must be taken to achieve high refractive index contrast relative to the GaN waveguide while maintaining low extinction coefficient.

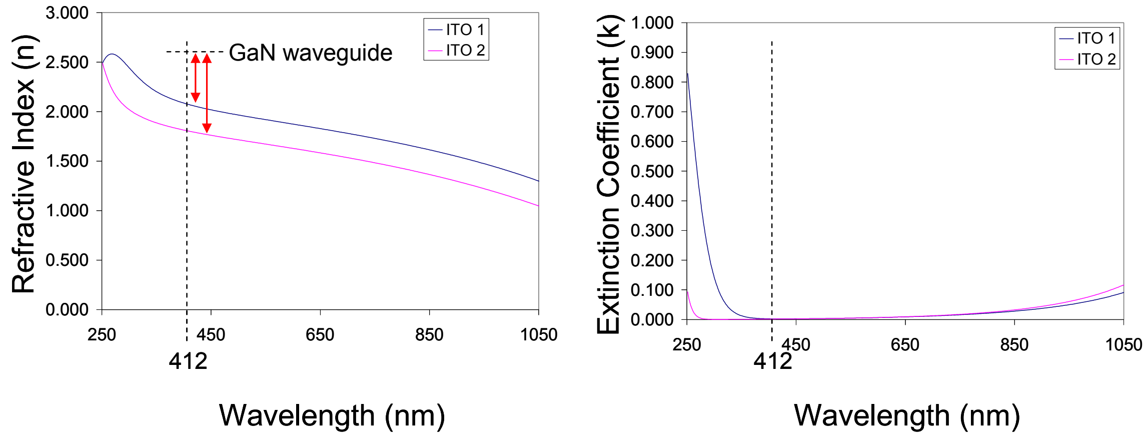

Figure 4: ITO refractive index and extinction coefficient under different ITO deposition conditions.

After ITO deposition, a low-temperature anneal was immediately performed to stabilize the film. The wafer was then annealed at a higher temperature to allow the ITO to form an ohmic contact with the underlying GaN. This step was followed by dry etching the ITO to form 120 µm-wide broad-area laser stripe patterns. Figure 5 shows the ITO sheet resistivity as a function of anneal temperature.

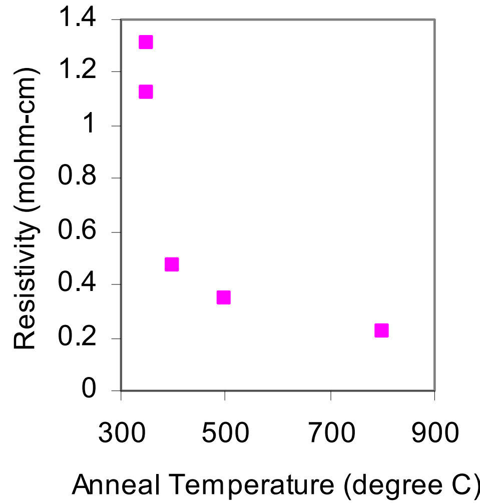

Figure 5: ITO refractive index and extinction coefficient under different deposition conditions.

Mesa structures aligned to the ITO stripes were formed by dry etching the heterostructure with Chemically-Assisted Ion Beam Etching (CAIBE). Laser facet mirrors for cavity lengths of 400, 500, 700, 1000, and 1500 µm were then patterned and etched with CAIBE. Finally, the n-contact pads and the upper electrodes were deposited by sequential thermal evaporation of Ti and Au.

The electrical and optical properties of the devices were evaluated. The current-voltage characteristics yielded a turn-on voltage of about 4.5V, with a slope resistance of about 65 ohms. The devices were evaluated at room temperature under pulsed conditions of 100 nsec pulse width and 1 kHz repetition rate. Figure 6 shows the light vs. current (L-I) characteristics of lasers with different cavity lengths. A plot of the threshold current density (Jth) as a function of cavity length is shown as an inset in the figure. Jth is relatively insensitive to length for long cavities because the distributed loss α dominates over the mirror loss. For short cavities, Jth increases rapidly with decreasing lengths because of the changing mirror loss, combined with a sublinear gain vs. current characteristic typical of quantum wells.

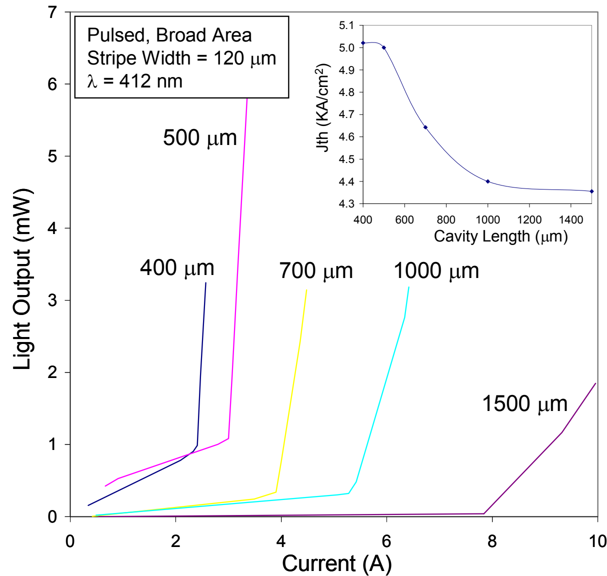

Figure 6: L-I Characteristics of broad area ITO-clad laser diodes.

The light spectrum peaked at λ = 412 nm, and experienced a sudden and sharp narrowing at threshold. As expected, a far-field interference pattern emerged at threshold, indicating spatial coherence upon lasing. This interference pattern results from the coherent combination of light coming from reflections off of the etched bottom surface area in front of the laser facet.

We also designed and demonstrated similar laser diode structures using other non-epitaxial cladding layers. In one structure, the ITO layer in Figure 2 was replaced with silver metal deposited by electron beam evaporation. Figure 7 shows the refractive index profile of the heterostructure, along with the optical mode profile. Silver was chosen as the waveguide cladding layer because of its high reflectivity at the lasing wavelength. Because of this property, the confined optical mode profile exhibits a very rapid decay into the silver at the silver/semiconductor interface. The shallow penetration depth of the electric field in the metal yields an acceptably low modal loss despite the high imaginary part of the index of refraction for Ag.

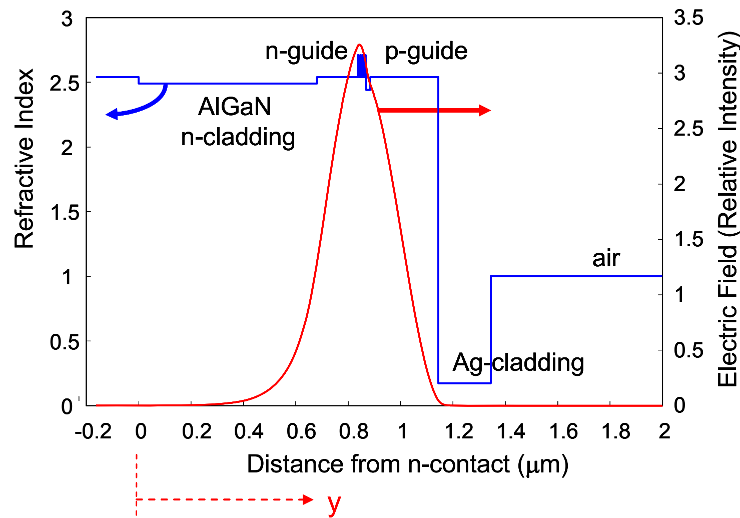

Figure 7: Optical mode profile in a silver-clad laser diode.

In another structure, the ITO layer in Figure 2 is replaced with a Ag-Pd-Cu alloy. The alloy is superior to pure Ag in terms of thermal stability, contact to p-GaN, and film adhesion. Figure 8 shows the L-I characteristics Ag-clad and Ag-Pd-Cu-clad LDs with different cavity lengths. The insets show the corresponding threshold current densities and the spectrum at I = 1.1 Ith, respectively. In addition to Ag and Ag-Pd-Cu, we have successfully demonstrated other cladding designs, such as one comprising a thin 13 nm-thick ITO phase matching layer paired with a 200 nm-thick Ag cap.

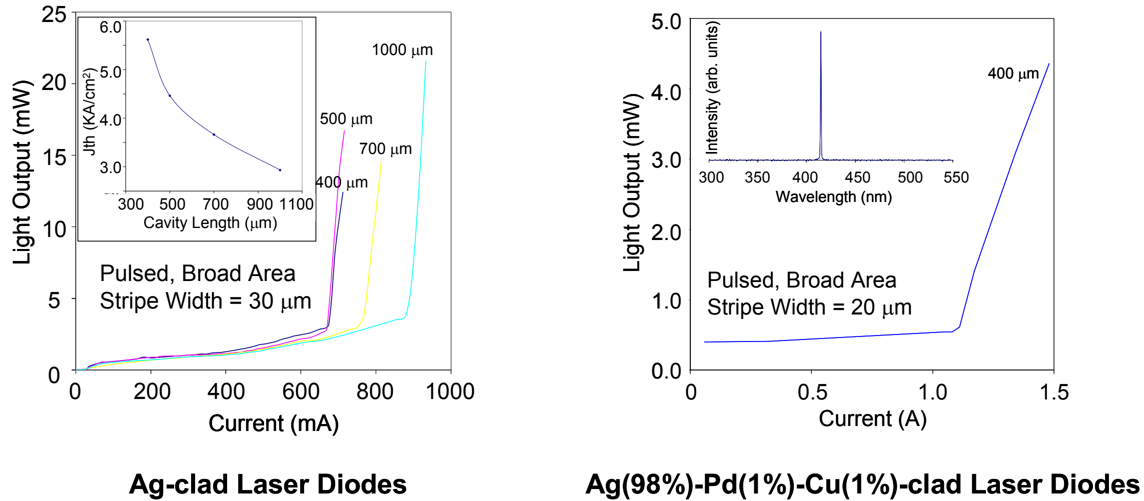

Figure 8: L-I characteristics of Ag and Ag-Pd-Cu-clad laser diodes.

In summary, we have described and demonstrated nitride laser diode structures utilizing non-epitaxial upper cladding layers. These materials perform effectively as cladding layers because of their unique optical and electrical properties. Non-epitaxial cladding layers provide an extra degree of freedom to semiconductor laser diode design, and promise to provide advantages such as improved current spreading, higher modal gain, ease of device processing, and reduced thermal load to sensitive active layers.

2. ULTRAVIOLET LIGHT EMITTING DIODES

AlGaN-based ultraviolet light emitting diodes have recently received wide interest because of their potential applications in ink and adhesive curing, bioagent detection, and germicidal eradication. The UV-A wavelength range of 315 to 400 nm are particularly suitable for UV curing because mature UV photoinitiators such as Irgacure 379 are available in this wavelength range. Moreover, highly efficient UV-A LEDs are already commercially available. Unlike mercury lamps, LEDs emit light in a single wavelength, so all the light energy is channeled to the wavelength needed for curing. The infra-red wavelength components in mercury lamps waste energy and cause heating problems.

The UV-B wavelength range of 280 nm to 315 nm is useful for medical phototherapy and bio-agent detection applications, as many biological molecules are spectroscopically sensitive to this wavelength range. The main applications of the UV-C wavelength range of 200 nm to 280 nm are those related to germicidal eradication, such as air purification or water disinfection. At sufficient intensities, light in this wavelength range damages the genetic materials of pathogens.

PARC has developed AlGaN-based MQW LEDs targeted at the UV-A wavelength range of 325 nm and at the UV-B wavelength range of 290 nm. The λ = 325 nm LED heterostructures have nominal Al alloy compositions of about 33%, while those for λ = 290 nm LEDs have nominal compositions of about 53%. Both structures use sapphire substrates and emit light through the substrate. Figure 9 shows the L-I characteristics of the devices when measured on wafer with no heat sink or any type of packaging.

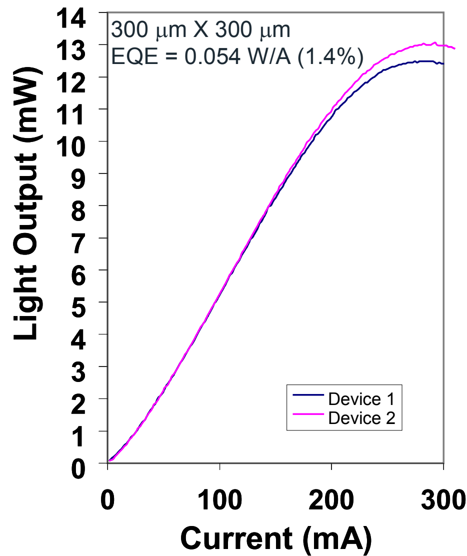

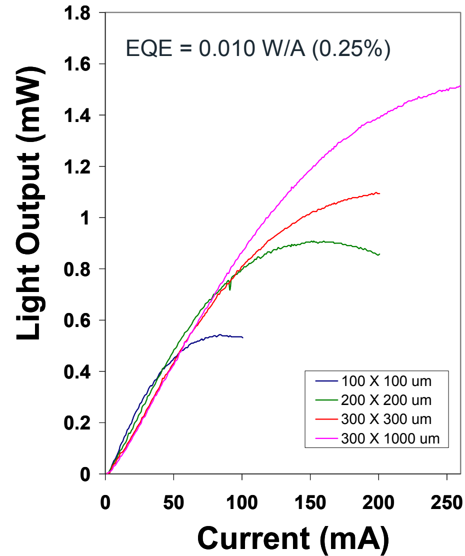

λ = 325 nm LED   λ = 290 nm LED

Figure 9: L-I wafer-level unpackaged characteristics of λ = 325 and λ = 290 nm LEDs.

UV LEDs with 300 micron square geometries operating at λ = 325 nm exhibit output powers of 13 mW with differential quantum efficiencies of 0.054 W/A measured under wafer-level, unpackaged condition with no heat sink. LEDs operating at λ = 290 nm under similar test conditions display output powers of 1.6 mW for large-area 300 μm X 1 mm devices.

ACKNOWLEDGEMENTS:

We thank the Army Research Laboratory (ARL) for collaboration in materials characterization, device processing, and device evaluation. The research was partially funded under the DARPA VIGIL and DTRA TAC-BIO programs.

REFERENCES:

[1] Bour et. al., Appl. Phys. Lett. **94**, 041124 (2009).
[2] Cheng et. al., IEEE Photon. Technol. Lett., **22** (2010).
[3] Strittmatter et. al., Phys. Status Solidi C, **DOI** 10.1002/pssc.200983557 (2010).